Electronic structure of silver overlayers on W(100)

A. Derraa
Department of Physics, University of Toronto, Toronto, Canada M5S 1A7

M. J. G. Lee
Department of Physics and Scarborough College, University of Toronto, Toronto, Canada M5S 1A7

(Received 6 November 1995)

The electronic structure of silver adsorbed on the (100) facet of a tungsten field emitter in the range of coverage from zero to three monolayers has been studied experimentally by means of field and photofield emission spectroscopy. An analysis of work function and total emission current data yields evidence that adsorbed silver reduces the surface density of states at the Fermi energy. It is found that adsorbed silver both suppresses the Swanson hump in the surface density of states of clean W(100) and also induces additional structures that depend largely on the number of complete overlayers. The experimental observations are interpreted by means of self-consistent fully relativistic supercell calculations of the layer densities of electronic states at the tungsten–vacuum and at the tungsten–silver–vacuum interface. The calculations predict silver-induced features in the surface density of states that are generally consistent with the experimental observations.

I. INTRODUCTION

Metallic overlayers on transition metal substrates are of great practical importance because of their relevance to electron emission devices and heterogeneous catalysis. Yet, with the exception of the alkali metals, the electronic properties of metallic overlayers on transition metal substrates have received little attention, perhaps because of the complexity of their electronic configurations. The W(100) surface of tungsten is of particular interest because it shows a rich complex of surface states and resonances lying close to the Fermi level.[1] Even though W(100) is among the most studied of the transition metal surfaces, little is known about the electronic structure of metallic overlayers adsorbed at a W(100)–vacuum interface. The present paper reports the results of an investigation of silver adsorbed on W(100) by means of electron emission spectroscopy.

Field emission spectroscopy is a surface-sensitive technique that can provide information about the occupied electronic states in the vicinity of the Fermi level, while photoemission spectroscopy is widely used to investigate the electronic structures of metals both below the Fermi level and above the vacuum level. Electronic states that lie between the Fermi level and the vacuum level are not accessible by either of these techniques. States in this energy range can be studied by means of inverse photoemission spectroscopy, which involves injecting electrons above the vacuum level and measuring the energy of the photon that is emitted when the electron drops to an unoccupied state between the Fermi level and the vacuum level. However, the inverse photoemission signal is extremely weak because the cross section of the inverse photoemission process is much smaller than that of the direct process. Moreover, in the presence of an adsorbate overlayer the inverse photoemission signal is superimposed on a background from the substrate, and it is difficult to extract the surface component of the signal.

Photofield emission, measured in conjunction with field emission, is an alternative means of probing the electronic states of the surface that lie between the Fermi level and the vacuum level. The sample is illuminated with p-polarized light having a photon energy smaller than the work function, and a strong static electric field is applied at the surface. Singly photoexcited electrons escape from the metal either by tunnelling through the surface potential barrier or by passing above it. Features in the total energy distribution of electrons emitted at the substrate–adsorbate–vacuum interface yield information about the electronic structure in the vicinity of E_F,[2–4] while their dependences on the photon energy make it possible to distinguish unambiguously between initial and final state structures. In addition, combined field and photofield emission measurements make it possible to determine independently the field factor and the work function at the emitting surface, yielding information about the profile of the adsorbate.[5]

Early calculations of the electronic structures of adatom–substrate complexes were based on the jellium model, in which the discrete ion cores of the substrate are smeared out into a uniform positive background charge. Although the jellium model is a useful starting point for evaluating quantities that depend on the distribution of charge only in an average way, this simplified model is not expected to describe adequately those adsorption phenomena that depend on the geometry of the substrate and on the d electrons of transition metals. Recently, some progress has been made in carrying out more realistic calculations in which the substrate is modeled by a slab consisting of a few atomic layers of the bulk material, with an ordered overlayer or overlayers on each side.[6–10]

The purpose of the present paper is to report an investigation of silver adsorbed on W(100) in the range of coverage from 0 to 3 ML (monolayers). It is found that 1 ML of adsorbed silver both suppresses the Swanson hump in the surface density of states of clean W(100) at 0.35 eV below

E_F, and also induces additional structures 0.70 eV below E_F and 2.3 eV above E_F. Above 2 ML these structures are replaced by a single structure centered above the Fermi level and extending to about 0.03 eV below E_F. Self-consistent fully relativistic energy band calculations have been carried out for the W(100)–vacuum and W(100)–silver–vacuum interfaces. The results of these calculations are compared with field emission, photofield emission, and photoemission data. It is concluded that the silver-induced features observed in field and photofield emission correspond to surface states and resonances of the substrate whose wave functions extend into, and are enhanced by, the silver overlayer.

The remainder of this paper is organized as follows. Section II is a brief description of the experimental apparatus and the method of data analysis. The experimental results are presented in Sec. III and discussed in Sec. IV. Section V is a summary of the results and conclusions of the present work.

II. EXPERIMENTAL

A. Apparatus and experimental procedure

The field and photofield emission spectrometer has been described in detail elsewhere,[11] as have the experimental chamber that contains the field emitter and the energy analyzer, and the deposition chamber that contains the Knudsen cell that serves as the atomic beam source.[12] The Knudsen cell is loaded with clean 99.99% pure silver and outgassed at 900 °C for no less than 24 h, after which the silver source can be operated at up to 1100 °C. The two chambers are independently pumped and interconnected by a duct fitted with a gate valve and a 1-mm-diam aperture. The aperture serves both to restrict the conductance between the chambers during deposition in order to minimize contamination of the tip by outgassing from the Knudsen cell, and to collimate the atomic beam to an angular width of less than 1°. With this arrangement, the base pressure in the experimental chamber remains below 10^{-10} Torr even when, during deposition, the pressure in the deposition chamber rises to 10^{-8} Torr.

A tungsten field emitter is mounted on a sample holder about 5 cm from a fluorescent conducting screen. The tip is grounded, and the potential difference between the tip and the screen is maintained at several kilovolts. The beam of electrons emitted from a single facet is selected by electrostatically deflecting the field emission pattern so that the image of the desired facet is centred over a small probe hole in the middle of the fluorescent screen. Electrons that pass through the probe hole enter a double-pass cylindrical energy analyzer, and electrons with energy within the selected range are detected by means of a spiraltron electron multiplier. The laser illumination system and related optics are all mounted outside the vacuum chamber. The apparatus is controlled by means of a PC-based data acquisition system.

Prior to deposition the field emitter was cleaned by flashing to incandescence, and both Fowler–Nordheim (FN) data (measurements of the total emission current from a single facet as a function of the tip-to-screen potential difference) and total energy distribution (TED) data for the clean facet were recorded. The silver flux was measured by means of a quartz crystal monitor mounted at right angles to the direction of the atomic beam, and the exposure was calculated from the dimensions of the apparatus and the angle of incidence on the emitting facet. To estimate the coverage from the exposure, a sticking coefficient of unity was assumed.[13] The Knudsen cell was operated at 1100 °C, at which temperature the vapour pressure of silver is approximately 3×10^{-2} mm Hg. Silver atoms were deposited at very low flux (typically 0.1 ML/min) on to the W(100) facet. The potential difference between the tip and the screen was held constant during deposition, and the emission current from the centre of the (100) facet was monitored continuously. Once the desired coverage had been reached, Fowler–Nordheim (FN) data were taken both in field emission and in photofield emission by sweeping the tip-to-screen potential difference through 100 channels each of width 5 V. The sweep sequence was repeated (typically 50 times) until adequate statistics had been achieved. Fowler–Nordheim data in photofield emission were acquired at fields sufficiently weak that the field emission component of the total emission current was negligible.

Finally, the total energy distributions (TED's) in field emission and in photofield emission were recorded. The tip bias voltage was swept through 100 channels, each of width 25 mV, spanning the appropriate energy range, the tip-to-screen potential difference being held constant. At each channel, the bias voltage was allowed to stabilize for 10 μs, then the detected electrons were counted for 500 μs. The sweep sequence was repeated, typically for 1000 cycles in field emission and for 2000 cycles in photofield emission, until adequate statistics had been achieved. All of the measurements were carried out at room temperature, and the tip was illuminated with p-polarized light at a large angle of incidence in order to enhance surface photoexcitation in photofield emission.[14]

Once all of the measurements at a given adsorbate coverage were complete, the tip was repeatedly flashed to remove the silver overlayer, and silver was deposited to the next exposure. The very high reproducibility of the dependence of the total emission current on deposition time demonstrated that throughout the experiment the silver flux was very stable.

B. Data analysis

The first step in the analysis of the data was to extract the work function ϕ from a Fowler–Nordheim plot of the total emission current measured as a function of the tip-to-screen potential difference. The electric field F at the tip is related to the potential difference between the tip and the screen V_{TS} by the relation $F=\beta V_{\mathrm{TS}}$, where the field factor β is the effective curvature of the hemispherical endform of the tip. The work function of the clean W(100) facet was taken to be 4.63 eV (based upon previous measurements on samples of macroscopic size)[15] and β was calculated by fitting the slope of a Fowler–Nordheim plot of the total emission current data [a plot of $\ln(I/V_{\mathrm{TS}}^2)$ against I/V_{TS}] to the theoretical slope $S_{\mathrm{FN}}(T)$ which is given by[5]

$$S_{\mathrm{FN}}(T)=-\tfrac{3}{4}(m/\hbar^2)^{1/2}\phi^{3/2}s(y)/\beta e + (8\pi^2k_B^2m_B/3\hbar^2e^2)T^2\phi t^2(y)/\beta V_{\mathrm{TS}}, \quad (1)$$

where e and m are the electronic charge and mass, k_B is Boltzmann's constant, T is the absolute temperature, and

$t(y)$ and $s(y)$ are slowly varying functions of $y=(e^3F)^{1/2}/\phi$ that are tabulated in the literature.[16] In the field range over which the present data were acquired (0.15–0.30 V/Å) the second term in Eq. (1) is very small compared to the first term, and the criterion for fitting a straight line to a Fowler–Nordheim plot of the experimental data and deducing β by interpreting the slope on the basis of Eq. (1) is well satisfied. Profile studies have shown that the field factor β of W(100) is not significantly changed by the presence of the adsorbate.[12]

Features in the surface density of electronic states at a metal–adsorbate–vacuum interface can be identified by comparing the experimental energy distribution $j(E)$ with the calculated free-electron distribution $j_0(E)$. The experimental distribution $j(E)$ decreases exponentially both below the Fermi energy E_F, due to the increasing thickness of the surface potential barrier, and above E_F, due to the decreasing probability of occupation of electronic states as described by the Fermi–Dirac distribution function. It is convenient to remove these irrelevant dependences by expressing the measured distributions in the form of an enhancement factor $R(E)$, which is defined by

$$R(E)=j(E)/[j_0(E)\otimes\Delta(E)], \tag{2}$$

where the denominator is the convolution of $j_0(E)$, the total energy distribution calculated from the free-electron model, with $\Delta(E)$, the Gaussian instrumental resolution function of the energy analyzer. The enhancement factor involves an undetermined multiplicative constant, because neither the area of the emitting surface sampled by the probe hole nor the collection efficiency of the energy analyzer is determined in the present work. It is convenient to remove the effect of this unknown constant by plotting $\ln R$ as function of energy.

The total energy distribution in photofield emission is similar in shape to that in field emission, but the peak in photofield emission occurs at $E_F+\hbar\omega$, where $\hbar\omega$ is the photon energy. The enhancement factor in photofield emission was deduced by dividing the observed total energy distribution in photofield emission by the convolution of the free electron distribution with the resolution function of the energy analyzer, as in Eq. (2). The free electron distribution in photofield emission was evaluated numerically using results that have been reported elsewhere.[12,17]

III. RESULTS

A. Work function as a function of exposure

In Fig. 1, the experimental points show the variation of the work function ϕ with silver exposure as determined from Fowler–Nordheim plots of the total field emission current data. The exposure is expressed in monolayers, where 1 ML corresponds to a single (1×1) overlayer of silver on W(100). In the range from zero to 1 ML, the work function decreases almost linearly with increasing exposure. It passes through a minimum at about 1 ML, increases, passes through a broad maximum, then decreases again. Above 2.5-ML exposure, the noise in the emission current due to fluctuations in the overlayer becomes sufficiently large that the present technique does not yield a reliable estimate of the work function.

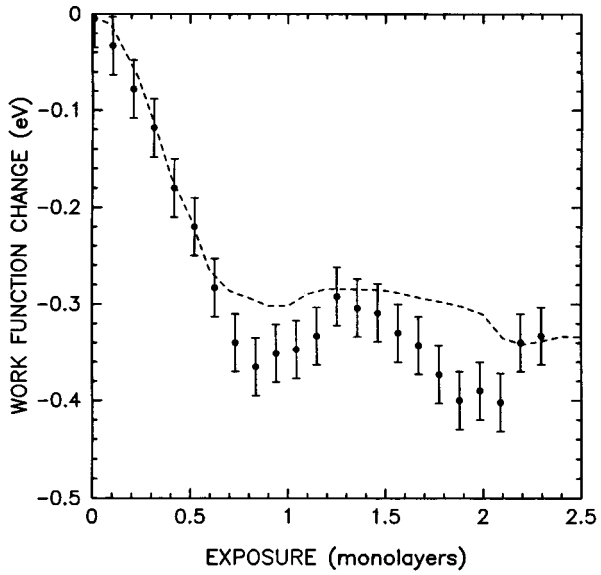

FIG. 1. The measured change in the work function at the center of the (100) facet of a tungsten field emitter at 300 K as a function of silver exposure. The dashed curve shows the variation in the work function that was calculated from the total emission current data assuming that in the range from 0.5 to 2.5 ML the density of surface states is constant. For reasons discussed in text, the discrepancies close to 1 and 2 ML are attributed to suppression of the surface density of states by the silver overlayer.

B. Total emission current as a function of exposure

Figure 2 shows the exposure dependence of the total emission current from the central region of the (100) plane, the potential difference between the tip and the screen being held constant. Initially the emission current decreases, pass-

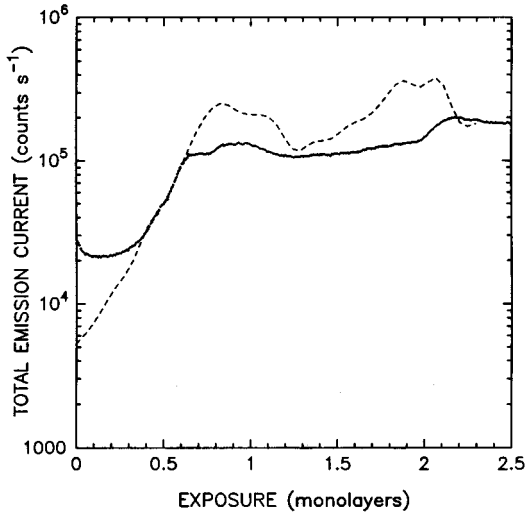

FIG. 2. The solid curve shows the total field emission current from the center of the W(100) facet of a tungsten field emitter in a field of 0.214 V Å^{-1} at 300 K, plotted as a function of silver exposure. The dashed curve is the exposure dependence of the total emission current calculated from the measured work function on the assumption that the surface density of states is independent of exposure. The discrepancies are attributed to suppression of the surface density of states by the silver overlayer. The emission current is plotted on a logarithmic scale.

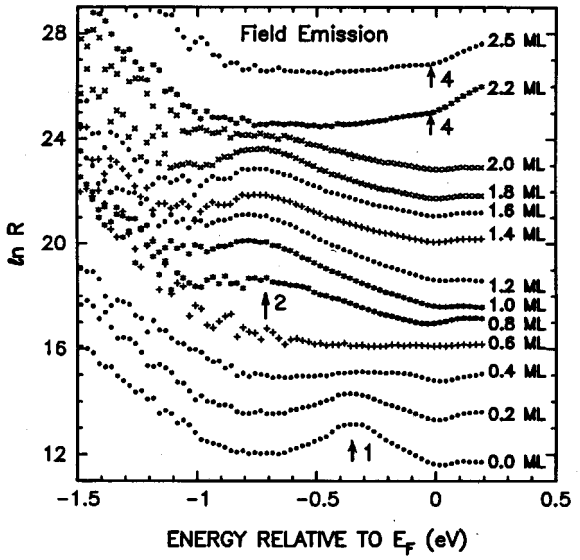

FIG. 3. Semilogarithmic plot of the enhancement factor R for field emission at 300 K from the center of the (100) facet of tungsten. Each curve is labeled by the silver exposure expressed in monolayers. The curves have been displaced vertically for clarity. The labeled arrows mark features in the observed spectra as discussed in the text.

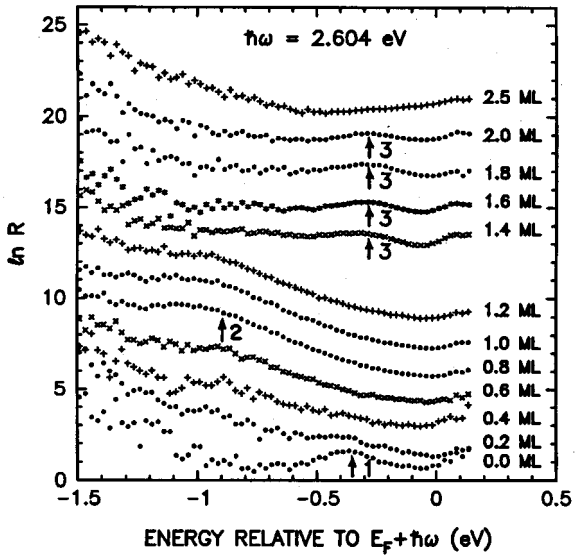

FIG. 4. Semilogarithmic plot of the enhancement factor R measured at 300 K for photofield emission from W(100) with a photon energy of 2.604 eV. Each curve is labeled by the silver exposure expressed in monolayers. The curves have been displaced vertically for clarity.

ing through a broad minimum at 0.5 ML, and then increasing rapidly toward a maximum almost three times the clean value. In the 1-ML to 2-ML range the behavior of the emission current is qualitatively similar to that in the zero to 1-ML range. Above 2 ML the emission current decreases steadily with increasing exposure and shows large fluctuations. Above 2.5 ML the fluctuations in the emission current are sufficiently large that measurements of the total emission current are not reproducible.

C. Enhancement factors

Field emission enhancement factors for a range of exposures of silver on W(100) are displayed in Fig. 3. The distribution from clean W(100) is dominated by the Swanson hump, which appears as a broad peak (marked by arrow 1 in Fig. 3) centered 0.35 eV below E_F.[18] With increasing exposure the Swanson hump is attenuated; it is completely quenched at one-half monolayer.

At an exposure of 0.7 ML, a broad peak (marked by arrow 2 in Fig. 3) appears at about 0.70 eV below E_F. This peak remains unchanged in height and width until the second monolayer is complete, then it disappears abruptly. In contrast to the Swanson hump, this peak is not at all sensitive to surface contamination; in a vacuum chamber at 10^{-10} Torr it remains unchanged for several weeks. Neither the height nor the width of this peak is affected by heating so long as the temperature is not sufficiently high to desorb the silver overlayer. As the exposure is increased above 2 ML, a discontinuity appears in the slope of the enhancement factor about 0.03 eV below the Fermi level (marked by arrow 4 in Fig. 3). Above about 2.5 ML the silver overlayer becomes unstable, and the total energy distributions are no longer reproducible.

Figures 4 and 5 show the photofield emission enhancement factors at photon energies of 2.604 and 3.049 eV, respectively. The quenching of the Swanson hump shows up in the photofield emission data, as does a broad silver-induced peak centred about 0.90 eV (for $\hbar\omega$=2.604 eV) and 0.80 eV (for $\hbar\omega$=3.049 eV) below the Fermi level. The breadth of this peak, together with the slight dependence of the initial state energy on the photon energy, suggest that it is due to electrons photoexcited from a range of initial states.

Two features that are not present in the field emission spectra show up in the photofield emission spectra. Firstly, in the range of exposure from 0.2 ML to above 1.0 ML, the

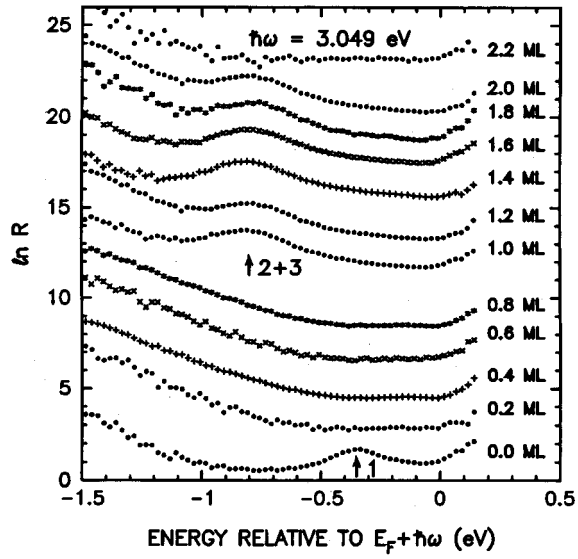

FIG. 5. Semilogarithmic plot of the enhancement factor R measured at 300 K for photofield emission from W(100) with a photon energy of 3.049 eV. Each curve is labeled by the silver exposure expressed in monolayers. The curves have been displaced vertically for clarity.

enhancement factors increase significantly as the total energy decreases from the Fermi energy to 0.8 eV below E_F. In addition, above 1-ML exposure the 2.604-eV distribution flattens and a new peak appears about 2.3 eV above E_F (marked by arrow 3 in Fig. 4). The absence of a similar peak in the field emission spectra is a strong indication that the peak represents structure in the density of final states. Unfortunately, any final state structure at this energy cannot be detected unambiguously in the 3.049-eV data, because it is too close in energy to the final state for transitions from the initial state resonance at 0.70 eV below E_F. Above 1.4 ML the initial state structure at 0.70 eV below E_F can not be resolved in the data at 2.604 eV. This might be because its energy distribution overlaps that of the final state structure at 2.3 eV. For exposures greater than 2 ML, the photofield emission enhancement factors are found to be featureless and similar to the enhancement factors in field emission.

IV. DISCUSSION

A. Total tunneling current and the work function

LEED studies[13] have shown that at room temperature a nonannealed 1-ML silver overlayer W(100) has a (1×1) structure. Since at room temperature the sticking coefficient for silver on W(100) is close to unity,[13] one silver adatom is deposited for each tungsten atom of the substrate at an exposure of 1 ML, so monolayer exposure corresponds closely to monolayer coverage.

The observed dependence of the work function on silver coverage (Fig. 1) can be related to the structure of the adsorbate overlayer. The lateral distance between adjacent adsorption sites on clean W(100) (3.16 Å) is comparable to the atomic diameter of silver (3.20 Å).[19] This suggests that silver will not fit easily into the hollows of the substrate, and that silver-covered W(100) may be less smooth than clean W(100). If this is so, the work function would be expected to decrease with increasing coverage.[20] Any transfer of charge from the silver overlayer to the substrate would also cause the work function to decrease with increasing coverage. These mechanisms are both consistent with the experimental finding that, in the system Ag/W(100), the work function decreases as the coverage increases from 0 to 1 ML. It is interesting to note that, at room temperature and in the range of coverage from 0 to 1 ML, both copper and gold absorbates increase the work function.[21–23] This may be because the atomic diameters of copper and gold are both significantly smaller than that of silver.[19]

In the range of coverage from 0 to 0.2 ML, the work function and the total emission current both decrease. As the observed decrease in the work function would be expected to increase the emission current, the observed decrease in the emission current is evidence that adsorbed silver decreases the surface density of electronic states. The dashed curve in Fig. 2 is a plot of the coverage dependence of the total emission current calculated from the work function data on the assumption that the surface density of states is independent of coverage. From the departure from the measured total emission current in the range of coverage from 0 to 0.5 ML, it is estimated that over this range of coverage adsorbed silver suppresses the surface density of states in the vicinity of the Fermi level by a factor of 5.1, of which only a small fraction (approximately 28%) is attributable to the quenching of the Swanson hump. Other, albeit smaller, discrepancies occur close to 1- and 2-ML coverage. The dashed curve in Fig. 1 is the coverage dependence of the work function that would bring the emission current calculated on the assumption of a constant surface density of states into agreement with the experimental data. As the discrepancies at 1- and 2-ML coverage are significantly larger than the experimental error in the work function, they are probably due to suppression of the surface density of states by the silver overlayer rather than to experimental error in the work function. From these data it is estimated that at coverages of 1 and 2 ML the surface densities of states in the vicinity of E_F are suppressed relative to that of clean W(100) by factors of 8.4 and 12.8, respectively.

The results of Bauer *et al.*[13] and of Kalaczkiewiez and Sidorski[24] for the work function change brought about by silver deposited at low coverage on a macroscopic W(100) surface are qualitatively similar to those reported here. The small discrepancies might be due to differences between microscopic and macroscopic facets. Takeda,[25] Jones,[26] and Centronio and Jones[27] have all reported that the average work function deduced from the whole tip emission current increases with increasing coverage of silver. However, it would be meaningless to compare the present data with the results of whole tip work function measurements, as in these latter measurements the current is dominated by emission from the facet on which the work function is lowest.

B. Electronic structure

An overlayer of adsorbed silver modifies the electronic structure of the tungsten–vacuum interface not only by quenching the Swanson hump (marked by arrow 1 in Figs. 3–5) but also by introducing new features in the observed enhancement factors. First, in the range of coverage from 0.7 to 2.0 ML, a strong initial-state peak centered about 0.70 eV below the Fermi level (marked by arrow 2) is observed both in field emission and in photofield emission. Second, in the range of coverage from 1.4 to 2 ML, a weak final-state peak 2.3 eV above E_F (marked by arrow 3) is observed in photofield emission at 2.604 eV. Third, above 2-ML coverage the slope of the field emission enhancement factor increases substantially about 0.03 eV below the Fermi level (marked by arrow 4), and all other structures in the enhancement factors disappear.

Broadening of the electronic levels of adsorbed silver into bands depends upon the existence of an ordered overlayer. The peak 0.70 eV below E_F (marked by arrow 2 in Figs. 3–5) has been observed with as little as 0.7-ML coverage of silver. In principle, island formation might result in an ordered overlayer below monolayer coverage, but there is no evidence for island formation in Ag/W(100) at room temperature. It is therefore unlikely that this peak is attributable to the valence states of the adsorbed silver atoms. Increasing silver coverage would be expected to modify the Ag–W and Ag–Ag interactions, so the absence of any shift or broadening of the peak with increasing coverage is a further indication that it is not attributable to the adsorbate levels. For these reasons, it seems likely that it is attributable to a weak structure 0.70 eV below E_F that has previously been observed in field emission from clean W(100).[28] This structure

has been attributed to a surface resonance of odd symmetry, so the field emission current is expected to vanish at normal emission.[14] Unlike the Swanson hump, this resonance apparently extends into the silver overlayer, because emission can still be observed at 2-ML coverage where the applied electrostatic field at the tungsten substrate is expected to be screened out by the silver overlayer. This suggests that adsorbed silver induces a spatial redistribution of the electron density, enhancing the density of electronic states at the surface layer.

The experimental data show that, for a given number of complete overlayers, the energy-dependent structures in the observed spectra change little as the coverage is increased continuously. This finding suggests that the surface density of states of Ag/W(100) depends largely on the number of complete overlayers, and is a further indication that the silver-induced peaks observed at low coverage correspond to intrinsic electronic states of the W(100) substrate whose wave functions extend into, and are to some extent modified by, the silver overlayer.

The structure observed in field emission above 2-ML coverage (marked by arrow 4 in Fig. 3) is attributed to emission from a surface state of the silver overlayer centred above the Fermi level and extending to about 0.03 eV below E_F. It is believed to correspond to a known surface state about 0.15 eV below E_F on the (111) facet of bulk silver.[29,30] No similar structure is to be expected in the photofield emission data because these data do not extend to sufficiently high energy. A similar structure has been observed on Ag/W(110) above 2-ML coverage,[31] suggesting that the emission properties of a double overlayer of silver are largely independent of the substrate.

C. Comparison with electronic structure calculations

In order to gain a fuller understanding of the origins of the structures discussed above, the electronic structures of a W(100)–vacuum interface and of a W(100)–Ag(1×1)–vacuum interface have been calculated on the basis of realistic models of the interfaces. The W(100)–vacuum interface was represented by a tetragonal supercell containing nine layers of tungsten atoms and seven layers of initially empty (charge-free) cells. LEED studies[32] have shown that at room temperature the relaxation of the free tungsten surface (the reduction in the inter-layer spacing at the surface as compared with that in the bulk) is about 4–6 %. The calculations reported in detail here are for a surface layer relaxed by 4%. The size of the supercell is therefore $a\times a\times 7.96a$, where a is the conventional lattice parameter of bulk tungsten. Self-consistent calculations for the W(100)–vacuum interface have also been carried out assuming an unrelaxed surface. It is found that the relaxation of the surface layer by 4% has only a minor effect on the layer densities of states.

To represent the W(100)–silver–vacuum interface, a (1×1) overlayer of silver atoms was added to the lattice at each tungsten–vacuum interface. To allow for the larger atomic diameter of silver (3.20 Å for Ag as compared with 2.70 Å for W) (Ref. 19) the distance between the outer tungsten layer and the silver overlayer was taken to be 10% larger than that between adjacent tungsten layers in bulk tungsten, resulting in a supercell of size $a\times a\times 9.10a$. The electronic structure of the metal–adsorbate–vacuum interface was calculated by solving the Dirac equation self-consistently by means of the LMTO method of electronic structure calculation including combined corrections.[33] The potential was assumed to be spherically symmetric within each atomic sphere, and exchange and correlation were taken into account in the local-density approximation as formulated by von Barth and Hedin.[34]

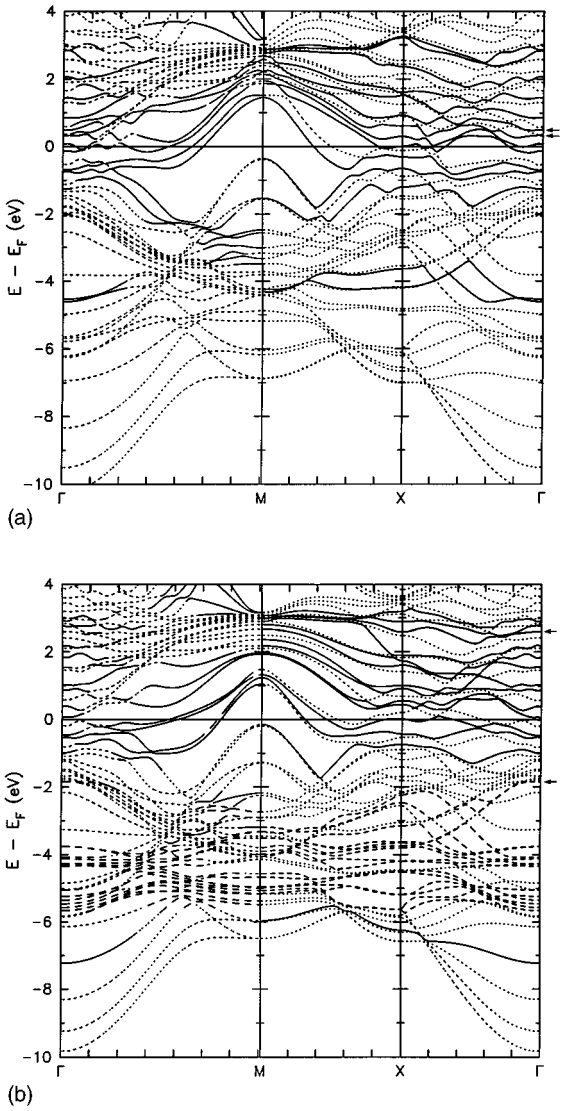

FIG. 6. Self-consistent fully relativistic electronic energy bands in the spherical potential approximation for supercells constructed to represent (a) a W(100)–vacuum interface, and (b) a W(100)–Ag–vacuum interface. The solid, dashed, and dotted lines denote those energy bands whose wave function amplitudes are largest in the outermost tungsten layer, in the silver overlayer, and in an inner tungsten layer, respectively. The arrows mark a pair of surface states that in the present approximation are almost degenerate in the absence of the silver overlayer.

The calculated energy bands of a W(100)–vacuum interface and a W(100)–Ag–vacuum interface in the principal symmetry directions are compared in Figs. 6(a) and 6(b). Those bands whose wave function amplitudes are largest in the silver overlayer and in the top tungsten layer are drawn with dashed and solid lines, respectively, and the remaining bands are drawn with dotted lines. The calculated energy

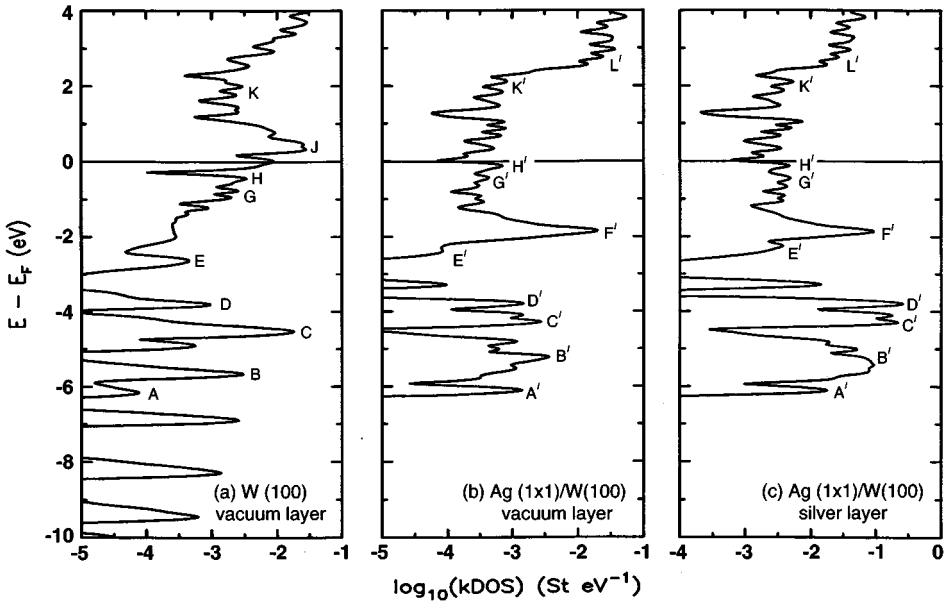

FIG. 7. Calculated **k**-resolved layer densities of states at Γ weighted by the barrier transmission factor appropriate to field emission (a) in the first vacuum layer of clean W(100), (b) in the first vacuum layer for W(100) with a (1×1) overlayer of silver, (c) in the silver overlayer for W(100) with a (1×1) overlayer of silver. Note the reduced layer density of states scale for curve (c).

bands of a W(100)–vacuum interface are in good overall agreement with bands deduced from electronic structure calculations for a nine-layer tungsten film.[35] As the number of valence electrons of silver (including the $4d$ electrons) is 11 and as there are two silver atoms per primitive unit cell of the superlattice, 11 additional bands are needed to accommodate the valence electrons of the silver overlayer. A comparison between the energy eigenvalues at Γ (the center of the surface Brillouin zone) shows that in the presence of the silver overlayer there are 12 additional eigenvalues below the Fermi level, with energies of −1.8 eV (two eigenvalues), −3.8 to −4.2 eV (4), −5.2 to −5.7 eV (5), and −7.2 eV (1). As only 11 bands are needed to accommodate the extra valence electrons, the silver overlayer lowers the Fermi energy by approximately 0.42 eV relative to the bottom of the band.

The present calculations for a clean W(100)–vacuum interface yield a closely spaced pair of surface states [marked by arrows in Fig. 6(a)] about 0.3 and 0.4 eV above the Fermi level. As the wave functions associated with these states are largely confined to the surface layer, it is not surprising that the energy difference between them does not depend significantly on the relaxation of the surface. However, in the presence of a 1×1 overlayer of silver one of these surface states moves below the Fermi level, contributing to the total of 12 silver-induced eigenvalues below the Fermi level, while the other moves to higher energy [marked by the arrows in Fig. 6(b)]. Unlike the other energy eigenvalues at Γ, these two eigenvalues prove to be very sensitive to the distance between the tungsten substrate and the silver overlayer. If the distance is taken to be equal to the inter-layer spacing in bulk tungsten, the surface states are 1.5 eV below E_F and 3.1 eV above E_F. If, as in the calculations reported in detail here, this distance is taken to be 10% greater than the interlayer spacing in bulk tungsten, the surface states are 1.8 eV below E_F and 2.6 eV above E_F.

In field and photofield emission, the tunneling barrier selects strongly for normal emission. Moreover, because the photon energy is smaller than the work function, photoexcitation in p-polarized light occurs predominantly in the region just outside the surface of the metal where the gradient of the normal component of the vector potential is large. Therefore, the emission currents in field emission and in photofield emission in p-polarized light are expected to be dominated by electrons from states whose wave functions are of large amplitude just outside the surface of the metal and whose **k** vectors lie close to the center of the surface Brillouin zone.

To facilitate comparison with experiment, both **k**-nonresolved and **k**-resolved densities of states have been computed for each layer of the supercell. The **k**-nonresolved layer densities of states were calculated by weighting the contributions of the various electron states in the surface Brillouin zone equally, and the **k**-resolved layer densities of states were calculated by weighting the contributions of the various electron states according to their relative probabilities of transmission through the Schottky barrier. The **k**-resolved densities of states in the first vacuum layer (the layer of initially empty cells that is closest to the surface layer) for a clean W(100) surface and for a (1×1) silver overlayer on W(100) are shown on semilogarithmic plots in Figs. 7(a) and 7(b), respectively. For comparison, the **k**-resolved density of states in the silver overlayer is plotted on a reduced scale in Fig. 7(b).

The **k**-resolved layer density of states in the first vacuum layer of a W(100)–vacuum interface shows features that are consistent with peaks in electron emission from a clean W(100) surface that have been observed experimentally at 0.35,[18] 0.70,[28] and 4.70 eV. (Ref. 23) below E_F. A comparison between Figs. 7(a), 7(b) and 7(c) shows that most of the features of the **k**-resolved density of states of the clean W(100) surface also appear in the layer densities of states at the W(100)–Ag–vacuum interface, both in the first vacuum layer and in the silver overlayer. In the presence of a silver overlayer, corresponding features of the layer densities of states [which are labelled by the same letter in Figs. 7(a), 7(b), and 7(c)] show up at slightly higher energies relative to the Fermi level than at the clean W(100)–vacuum interface as a consequence of the lowering of the Fermi level relative to the bottom of the band. In addition, the silver overlayer introduces several $4d$-like energy bands below the Fermi level [shown as dashed lines in Fig. 6(b)]. The strong peak

C' in the silver overlayer [Fig. 7(c)] corresponds to a group of four such d-like bands. That this peak is smaller by two orders of magnitude in the first vacuum layer than in the silver overlayer is evidence that the $4d$-like electrons of silver are highly localized and effectively confined to the silver overlayer by the centripetal potential.

In bulk tungsten, the Fermi level is close to a minimum in the density of states, but at a clean W(100)–vacuum interface the Fermi level is close to a maximum in the surface density of states.[36] The present calculations indicate that in the presence of a (1×1) silver overlayer the **k**-resolved surface density of states at the Fermi level is reduced by a factor of about 7.6 relative to that of the clean W(100)–vacuum interface. This is consistent with the factor of 8.3 that was inferred from the work function and total emission current data. It is known that a (1×1) copper overlayer on W(100) brings about a much larger reduction in the surface density of states.[37] The closely spaced pair of surface states on W(100) predicted by the present calculations [marked by the arrows in Fig. 6(a)] gives rise to a strong peak J in the **k**-resolved density of states about 0.35 eV above the Fermi level. Unfortunately, peak J is too high in energy to be resolved as a distinct peak in field emission and too low to be resolved in photofield emission, although transitions to J might contribute to the low energy tail of the photofield emission distribution at 2.604 eV. In the presence of a silver overlayer, one of the surface states is lowered in energy and the other is raised [marked by the arrows in Fig. 6(b)] The shifting of the surface states to F' and L' contributes to the reduction in the surface density of states at the Fermi energy that occurs in the presence of the silver overlayer.

The energy of the group of surface resonances K is such that in photofield emission spectra at 2.604 eV it would be impossible to distinguish between transitions to K and transitions from the initial state G. Together, these states are expected to yield a broad enhancement near 0.90 eV below E_F, as is observed experimentally (marked by arrow 2 in Fig. 4).

The silver-induced final state resonance that is observed experimentally at 2.3 eV above E_F is attributed to the surface state of higher energy that shows up as the strong edge L' in the **k**-resolved density of states. The coverage dependence of L' is consistent with the experimental data, but the energy (2.6 eV above E_F) is slightly too high. As the splitting of the surface states is found to be very sensitive to the spacing between the silver overlayer and the tungsten substrate, the slight discrepancy in energy suggests that the relaxation of the silver overlayer may be slightly larger than the figure of 10% assumed in the present calculations.

The Swanson hump 0.35 eV below the Fermi level (labeled by arrow 1 in Figs. 3–5) is a prominent feature of the experimental field and photofield emission spectra of a clean W(100) surface. Two surface resonances at Γ contribute to peak H of the calculated **k**-resolved surface density of states, which coincides in energy with the Swanson hump. In the presence of an overlayer of silver, the corresponding peak H' is weaker by an order of magnitude. This is consistent with the experimentally observed quenching of the Swanson hump by a monolayer overlayer of silver. However, the calculated peak does not dominate the **k**-resolved density of states to the same extent that emission from the Swanson hump dominates the experimental total energy distribution. The present calculations involve the assumption that the potential is spherically symmetric within each atomic sphere. The wave functions of the surface states of the W(100)–vacuum interface are essentially localized within a single atomic sphere, so the spherical potential approximation does not fully take into account the effect of the strong potential gradient at the interface. Beyond the spherical potential approximation, the potential gradient at the interface is expected to split the energies of the two surface states. If one of the surface states were to be lowered in energy to the region of the Swanson hump, the agreement between the **k**-resolved layer density of states and the experimental total energy distribution for the clean W(100)–vacuum interface would be greatly improved. In the presence of a silver overlayer the wave functions of the surface states extend over both the substrate and the overlayer, so the present spherical potential approximation is expected to yield a more accurate description of the electronic structure of the W(100)–silver–vacuum interface.

In the range of coverage from 0.8 to 2.0 ML, an initial-state peak (marked by arrow 2 in Figs. 3–5) is observed 0.70 eV below E_F both in field emission and in photofield emission. An initial-state peak has previously been reported in the same energy range in emission from a clean W(100)–vacuum interface,[28] but it is sufficiently weak in the absence of a silver overlayer that it was not detected in the present experiments. The experimental peak is close in energy to the pair of surface resonances G in the **k**-resolved density of states. However, the experimental data show that the silver overlayer enhances the emission current, whereas peak G in the **k**-resolved density of states is suppressed by a (1×1) silver overlayer. Peak G corresponds to a pair of surface resonances of odd symmetry with respect to reflection in a {100} plane normal to the surface. Being of odd symmetry, these resonances are orthogonal to a plane wave in the vacuum, so at a clean W(100)–vacuum interface their contribution to the current is expected to vanish at normal emission. It is suggested that inhomogeneities in the potential of the silver overlayer may couple substrate resonances of odd symmetry to plane waves in the vacuum, thereby enhancing their contributions to the emission current.

The present calculations predict that when a (1×1) silver overlayer is deposited on W(100), each silver atom loses 0.215 electrons as a result of charge transfer to the substrate. As is pointed out above, such a transfer of charge may contribute significantly to the experimentally observed decrease in the work function with increasing coverage of silver.

D. Comparison with published data

In field emission studies of Au/W(100), Richter and Gomer[21] have observed the Swanson hump at greater than 1-ML coverage. They attributed the persistence of the Swanson hump to the close similarity between the potential of the gold overlayer and that of the tungsten substrate. Billington and Rhodin[22] have reported that, in the presence of copper and gold adsorbates, emission peaks 0.35 and 0.80 eV below E_F appear at 0, 1, 2, and 3 ML, but are quenched at intermediate coverages. They interpreted their data on the basis of a model by Kar and Soven[38] according to which a peak may persist so long as the overlayer has (1×1) symmetry. The

present results for Ag/W(100) show not only that the Swanson hump is quenched at 1 and 2 ML coverage, but also that other resonances can be observed at intermediate coverages. Thus the argument of Kar and Soven suggests that in Ag/W(100) the potential of the silver overlayer is significantly different from that of the tungsten substrate. This may be because, unlike copper and gold, silver does not fit easily into the hollows of the W(100) substrate.

The present results can usefully be compared with the data of Attard and King[23] for photoemission from Ag/W(100). The most striking feature of their data for clean W(100) is a strong emission peak 0.37 eV below the Fermi level that is quenched by a 1-ML overlayer of silver. They also observed strong emission peaks from clean W(100) about 1.4 and 4.5 eV below E_F, while the present **k**-nonresolved density of states calculations in the first vacuum layer yield peaks 0.7, 2.1, 4.5, and 4.7 eV below the Fermi level. In photoemission from unannealed Ag/W(100) at monolayer coverage, Attard and King found peaks approximately 1.3, 2.6, 5.3, and 8.0 eV below E_F, while the present calculations predict a similar pattern of strong peaks somewhat shifted in energy, 0.8, 1.8, 4.0, 4.2, and 5.1 eV below E_F, together with a silver-induced surface resonance 7.0 eV below E_F (the peaks at 4.0 and 4.2 eV would not be expected to appear as distinct peaks in the photoemission data, as the experimental resolution is only about 0.5 eV). Attard and King did not detect the silver-induced emission peak, 0.7 eV below E_F, that is a strong feature of the present data. This peak, which has been attributed to an energy band of odd symmetry, is expected to be observed in photoemission only if there is a component of the electromagnetic field parallel to the surface. Thus, one possible reason for the difference between the present results and the photoemission data is the plane of polarization of light, which for the photoemission data was not reported. Another possible reason for differences between the spectral features observed in the two experiments is that in photofield emission the tunnelling barrier selects strongly for emission from electronic states that lie close to the center of the surface Brillouin zone. In photoemission the photon energy is also an important consideration, because for more highly localized states the photoexcitation probability tends to peak at a higher photon energy.[39]

V. CONCLUSIONS

A comparison between the coverage dependence of the work function and of the total emission current for a W(100)–vacuum interface offers evidence that adsorbed silver significantly reduces the surface density of electronic states. Unlike copper and gold on W(100), adsorbed silver is found to decrease the work function. It is argued that the large atomic diameter of silver means that adsorbed silver atoms cannot be accommodated in the hollows of the W(100) substrate, and that silver-induced roughening the W(100) facet together with charge transfer to the substrate account for the decrease in the work function with increasing coverage of silver.

Features in the energy dependence of the surface density of states of the (100) facet of a tungsten field emitter have been studied experimentally. It is found that 0.5-ML coverage of adsorbed silver is sufficient to quench the Swanson hump, and no reappearance of this state is detected at higher coverage. In the range of coverage from 1 to 2 ML, two silver-induced structures are observed, one corresponding to an initial state 0.70 eV below E_F and the other to a final state 2.3 eV above E_F. The data yield evidence that these structures correspond to intrinsic surface resonances of the W(100) substrate whose wave functions extend into the silver overlayer. A third silver-induced structure, apparently centered above the Fermi level and extending to about 0.03 eV below E_F, appears above 2 ML coverage. It is attributed to a surface state of the double silver overlayer.

The experimental data are compared with the predictions of self-consistent fully relativistic electronic structure calculations for clean W(100) and for W(100) with a (1×1) overlayer of silver. A peak in the calculated **k**-resolved layer densities of states is consistent in energy with the experimentally observed Swanson hump, but is relatively weak in intensity. It is suggested that this may be because the present spherical potential approximation underestimates the splitting in energy of a pair of surface states of the clean W(100)–vacuum interface. Further calculations are needed to investigate this possibility. The silver-induced final state peak observed 2.3 eV above the Fermi level is attributed to the surface state that is shifted to higher energy in the presence of the silver overlayer. It is suggested that coupling of substrate states of odd symmetry to plane wave states in the vacuum by inhomogeneities in the silver overlayer may account for the observed enhancement by silver of emission from intrinsic surface resonances of W(100) that lie approximately 0.7 eV below the Fermi energy.

This study demonstrates the usefulness of photofield emission spectroscopy for studying features in the surface density of states at a metal–adsorbate–vacuum interface, and of electronic structure calculations based on the supercell method as a guide to the interpretation of the data. The overall consistency between the experimental data and the results of the supercell calculations leads us to conclude that such calculations have much to contribute to a better understanding of the electronic structures of metal–vacuum and metal–adsorbate–vacuum interfaces.

ACKNOWLEDGMENTS

We are grateful to Dr. G. A. Gaudin for his help and for many fruitful discussions. We wish to thank Dr. V. I. Smelyansky for making the LMTO program available to us, and for help in adapting it to the layer calculations. The help of A. Gradinaru in performing the calculations of the coverage dependence of the total emission current and the suppression of the surface density of states is gratefully acknowledged. This work was supported in part by operating and equipment grants from the Natural Science and Engineering Research Council (NSERC) of Canada. One of us (A.D.) wishes to acknowledge partial financial support from the University of Toronto.

[1] A. Modinos, *Field, Thermionic, and Secondary Emission Spectroscopy* (Plenum, New York, 1984), Chap. 7.
[2] D. Venus and M. J. G. Lee, Phys. Rev. B **34**, 4449 (1986).
[3] T. Radon and S. Jaskolka, Surf. Sci. **200**, 199 (1988).
[4] T. Radon and S. Jaskolka, Surf. Sci. **231**, 160 (1990).
[5] G. Gaudin and M. J. G. Lee, Surf. Sci. **185**, 283 (1987).
[6] M. Posternak, H. Krakauer, A. J. Freeman, and D. D. Koelling, Phys. Rev. B **21**, 5601 (1980); L. F. Madhouse and D. R. Harmann, *ibid*. **29**, 5372 (1984).
[7] P. Soukiassian, R. Rican, J. Lecante, E. Wimmer, S. R. Chubb, and A. J. Freeman, Phys. Rev. B **31**, 4911 (1985).
[8] J. E. Houston, P. J. Feibelman, D. G. O'Neill, and D. R. Hamann, Phys. Rev. B **45**, 1811 (1992).
[9] J. E. Houston, C. H. F. Peden, P. J. Feibelman, and D. R. Hamann, Phys. Rev. Lett. **56**, 375 (1986); Surf. Sci. **192**, 457 (1987).
[10] J. E. Houston, J. M. White, P. J. Feibelman, and D. R. Hamann, Phys. Rev. B **38**, 12 164 (1988).
[11] D. Venus and M. J. G. Lee, Rev. Sci. Instrum. **56**, 1206 (1986).
[12] G. A. Gaudin and M. J. G. Lee, Surf. Sci. **280**, 91 (1993); **310**, 34 (1994); Phys. Rev. B **49**, 5575 (1994); G. A. Gaudin, Ph.D. thesis, University of Toronto, Toronto, 1993.
[13] E. Bauer, H. Poppa, G. Todd, and P. R. Davis, J. Appl. Phys. **48**, 3773 (1977).
[14] D. Venus and M. J. G. Lee, Surf. Sci. **125**, 452 (1983); **172**, 477 (1986).
[15] R. W. Strayer, W. Mackie, and L. W. Swanson, Surf. Sci. **34**, 225 (1973).
[16] J. W. Gadzuk and E. W. Plummer, Rev. Mod. Phys. **45**, 487 (1973).
[17] C. Schwartz and M. W. Cole, Surf. Sci. **115**, 290 (1982).
[18] L. W. Swanson and L. C. Crouser, Phys. Rev. Lett. **16**, 389 (1966).
[19] J. C. Slater, *Quantum Theory of Molecules and Solids* (McGraw-Hill, New York, 1965), Vol. 2, Chap. 2.
[20] R. Smoluchowski, Phys. Rev. **60**, 661 (1941).
[21] L. Richter and R. Gomer, Phys. Rev. Lett. **37**, 763 (1976).
[22] R. L. Billington and T. N. Rhodin, Phys. Rev. Lett. **41**, 1602 (1978).
[23] G. A. Attard and D. A. King, Surf. Sci. **222**, 351 (1989).
[24] J. Kolaczkiewicz and Z. Sidorski, Surf. Sci. **63**, 501 (1977).
[25] E. Sugata and K. Taketa, Phys. Status Solidi **38**, 549 (1970).
[26] J. P. Jones, Surf. Sci. **32**, 29 (1972).
[27] A. Centronio and J. P. Jones, Surf. Sci. **44**, 109 (1974).
[28] E. Plummer and J. W. Gadzuk, Phys. Rev. Lett. **25**, 1493 (1970).
[29] P. Hermann, H. Neddermeyer, and H. F. Roloff, J. Phys. C **10**, 617 (1977).
[30] G. V. Hanson and S. A. Flodstrom, Phys. Rev. B **17**, 473 (1978).
[31] A. Derraa and M. J. G. Lee, Surf. Sci. **329**, 1 (1995).
[32] M. K. Debe and D. A. King, Surf. Sci. **81**, 193 (1979); J. A. Walker, M. K. Debe, and D. A. King, *ibid*. **104**, 405 (1981).
[33] H. L. Skriver, *The LMTO Method* (Springer-Verlag, Berlin, 1984).
[34] U. von Barth and L. Hedin, J. Phys. C **5**, 1629 (1972).
[35] S. Ohnishi, A. J. Freeman, and E. Wimmer, Phys. Rev. B **29**, 5267 (1984).
[36] D. Singh and H. Krakauer, Surf. Sci. **216**, 303 (1989).
[37] G. Gaudin and M. J. G. Lee, Prog. Surf. Sci. **48**, 109 (1995).
[38] N. Kar and P. Soven, Solid State Comm. **20**, 977 (1976).
[39] W. C. Price, A. W. Potts, and D. G. Streets, in *Electron Spectroscopy*, edited by D. A. Shirley (North-Holland, New York, 1972), p. 182.